Phosphorus Molecules on Ge(001): A Playground for Controlled n-Doping of Germanium at High Densities

Giordano Mattoni,[†] Wolfgang M. Klesse,[‡] Giovanni Capellini,[§] Michelle Yvonne Simmons,[‡] and Giordano Scappucci[†,*]

[†]School of Physics, University of New South Wales, Sydney, NSW 2052, Australia, [‡]Australian Research Council of Excellence for Quantum Computation and Communication Technology, School of Physics, University of New South Wales, Sydney, NSW 2052, Australia, and [§]Dipartimento di Scienze, Università degli Studi Roma Tre, Viale G. Marconi 446, 00146 Roma, Italy

ABSTRACT The achievement of controlled high n-type doping in Ge will enable the fabrication of a number of innovative nanoelectronic and photonic devices. In this work, we present a combined scanning tunneling microscopy, secondary ions mass spectrometry, and magnetotransport study to understand the atomistic doping process of Ge by P_2 molecules. Harnessing the one-dimer footprint of P_2 molecules on the Ge(001) surface, we achieved the incorporation of a full P monolayer in Ge using a relatively low process temperature. The consequent formation of P—P dimers, however, limits electrical activation above a critical donor density corresponding to P—P spacing of less than a single dimer row. With this insight, tuning of doping parameters allows us to repeatedly stack such 2D P layers to achieve 3D electron densities up to $\sim 2 \times 10^{20}$ cm^{-3}.

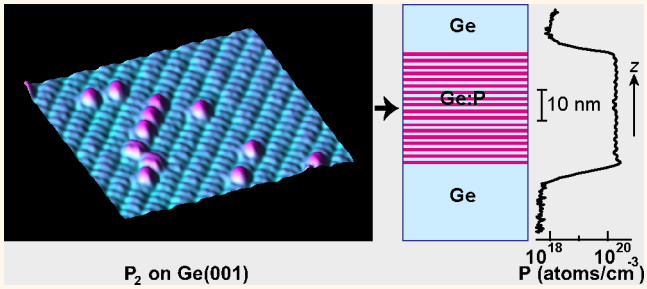

KEYWORDS: germanium · doping · laser · phosphorus · STM · magnetotransport

Merging electricity and light in one silicon chip will extend our ability to acquire, store, manipulate, and transmit information beyond the current limits imposed by transistor miniaturization. While optoelectronic devices such as photodetectors[1] and electro-optic modulators[2] have been integrated and mass-scale produced on the Si platform, the development of an industrially viable Si-integrated light source is still missing. Germanium is a promising candidate material to develop an integrated laser on silicon[3] by using both strain engineering to further decrease the small energy difference between the conduction valley at the Λ and Γ points and n-type doping to ease the achievement of population inversion and thus obtain net optical gain.[4]

However, after the pioneering demonstration of optically[5] and electrically[6] pumped lasing, the efforts in the development of an effective Ge-on-Si based laser have failed to date to increase the material gain and, consequently, reduce the unpractical high threshold current.[7] A recent theoretical analysis of the relative merits of strain *versus* doping toward the development of an efficient Ge-on-Si laser has in fact shown that an optimal doping level in the 10^{19}—10^{20} cm^{-3} range must be targeted for a particular strain level, with higher strain giving better lasing properties.[8] If the high-strain route is pursued toward the development of an industrially viable Ge-on-Si laser, then the ability to precisely control doping over a large range of densities is crucial to overcome loss mechanisms such as Auger recombination[9] and to control band gap narrowing,[10] ultimately increasing the gain at a given wavelength. As reviewed in ref 7, relatively large values of biaxial tensile strain have been recently reported in the literature. The achieved values, ranging in the 1—1.5% interval, together with an n-type doping density of 10^{19}—10^{20} cm^{-3} could gain values as high as 6000 cm^{-1} by injecting a relatively low density of excess carriers. As a consequence, lasing threshold current densities 3—4 orders

* Address correspondence to giordano.scappucci@unsw.edu.au.

Received for review October 4, 2013 and accepted November 11, 2013.

Published online November 11, 2013
10.1021/nn4051634

© 2013 American Chemical Society

of magnitude lower than that reported in ref 6 are to be expected.

Achieving high density n-doping of Ge in a controllable way is difficult using standard implantation techniques due to fast dopant diffusion and dopant solubility.[11−13] *In situ* doping techniques appear more promising, allowing high carrier activation while avoiding ion implantation damage and deactivation. Phosphorus is the most commonly used donor atom for applications; however, only PH_3 has been so far investigated in detail as a dopant precursor molecule.[14−20] Upon adsorption at room temperature on the Ge(001) surface, PH_3 dissociates into PH_2+H with a footprint of one dimer on the surface thus leading to a maximal coverage of half of a monolayer.[21] Previous studies have shown that incorporation of P donors at high density leads to dopant deactivation likely due to the formation of electrically inactive complexes such as P−P dimers.[22] Targeted experiments to validate this hypothesis have, however, not been performed to date.

Here we present a combined scanning tunneling microscopy (STM) and magnetotransport study into the doping process of Ge from phosphorus molecules (P_2) obtained from a GaP solid source upon thermal decomposition. Phosphorus molecules are an alternative choice as an n-type Ge dopant,[23] and from an application point of view, GaP solid sources are very convenient since they do not require particular handling procedures compared to the highly toxic phosphine gas. Moreover, previous studies have demonstrated the viability of P_2 for δ-doping of Si with electrical characteristics of the 2D-doped layers benchmarking those obtained using PH_3 in a similar doping process.[24]

RESULTS AND DISCUSSION

P_2 Adsorbates on Ge(001) and P Incorporation at Low Coverage. Figure 1a shows filled states of the Ge(001) after exposure at ∼100 °C to a low dose of P_2 (10 min) to identify the key adsorbate species formed. Figure 1b shows the surface after thermal anneal at 250 °C to drive incorporation of P atoms into the surface. Two distinct bright features appear in the postexposure image due to P_2 chemisorption, cumulatively accounting for 97% of the adsorbates on the surface ($P_{2,a}$ and $P_{2,b}$, red and yellow boxes, respectively).

In Figure 1c, we present a close-up image of a $P_{2,a}$ feature recorded in dual bias mode. $P_{2,a}$ is the most abundant species (population of ∼86%) and sits centered over two Ge dimers on the same dimer row with an apparent height against the dimer row average of ∼150 pm. We identify this feature as a P dimer with the orientation of the P−P bond perpendicular to the Ge dimer bond (Figure 1c, top view adsorption cartoon). This assignment is done in analogy with the P_2/Si(001) system,[25] where, among a total of four distinct structures of P dimer adsorbates, the P_2(I) species in ref 25 is

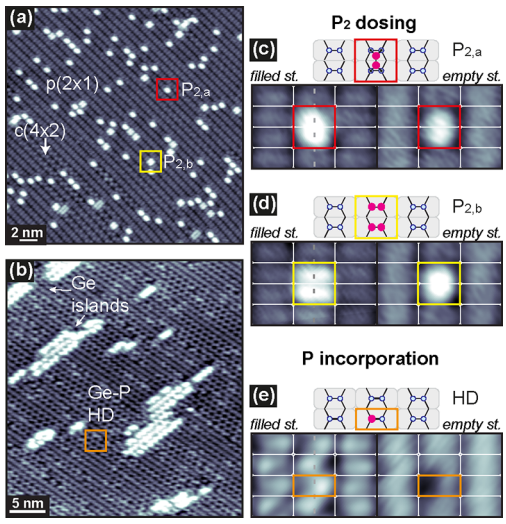

Figure 1. Low-coverage STM images of Ge(001) dosed with P_2: (a) 10 min exposure at T_{SUB} = 100 °C with $p(2 \times 1)$ and $c(4 \times 2)$ reconstruction visible and (b) after thermal anneal at T_{SUB} = 250 °C. Close-up dual bias images highlight the presence of different structures due to dosing: (c) most abundant $P_{2,a}$ species with the P−P bond perpendicular to Ge dimers and (d) $P_{2,b}$ with the bond parallel to Ge dimers. (e) Incorporated Ge:P heterodimers (HD) appear as zigzag features.

strikingly similar to the $P_{2,a}$ feature, albeit at a lower relative population of 52%. Because the P−P bond is oriented perpendicular to the Ge dimers, in this adsorption configuration, two P atoms are bonded to four Ge atoms arranged in consecutive dimers, thus potentially leading to a maximal coverage of 0.5 ML of P.

The $P_{2,b}$ structure (population of ∼11%), presented in Figure 1d, also occupies two dimers on the same dimer row but has a "butterfly-like" appearance in filled states and an apparent height against the dimer row average of ∼140 pm. In empty states, $P_{2,b}$ appears similar to $P_{2,a}$ although with a lesser surrounding halo. Although such a feature is not directly observed on the Si(001) surface, we speculate that $P_{2,b}$ arises from pairing of P_2 features similar to the P_2(II) species observed in ref 25. In our experiments, such pairing is likely promoted by the higher substrate temperature during P_2 dosing (∼100 °C *vs* room temperature in ref 25) and STM imaging (room temperature *vs* ∼−195 °C in ref 25). Because the P_2(II) feature in ref 25 is characterized by P−P bonds parallel to the Ge dimer, the $P_{2,b}$ structure allows for a full P monolayer at high coverages. A conclusive assignment of the $P_{2,b}$ feature requires detailed density functional theory simulations to test adsorption models of P_2 on Ge(001) and interactions of P_2-derived adsorbates and understand how these differ from the P_2/Si(001) system. However, our empirical interpretation is supported by STM characterization of dosed surface under high-coverage conditions and structural characterization by secondary ions mass spectroscopy (SIMS), as shown in the next sections.

Upon thermal annealing to 250 °C for 1 s (Figure 1b), we find that all products of P_2 chemisorption in low-coverage conditions have transformed and are no longer observed: only one single feature characterized by a bright zigzag appearance is present on the surface (Figure 1b, orange box). Two clues suggest that the zigzag feature is the Ge−P heterodimer (HD) arising from P incorporation into the Ge(001) surface. First, its appearance in both filled and empty states at high biases (Figure 1e) is strikingly similar to the well-studied Si−P heterodimer.[26] In filled states, a bright protrusion is observed at one dimer end with strong buckling of neighboring Ge atoms, which are bright also empty states. The second signature of P incorporation is the formation of elongated 2D islands (Figure 1b) made of Ge atoms as observed in previous PH_3/Ge(001) studies.[27] P incorporates into Ge(001) ejecting Ge adatoms which diffuse preferentially along dimer rows and aggregate into elongated 2D islands.

Saturation Dosing and Near-Monolayer Coverage. Moving on from low-coverage dosing and isolated adsorbates, we now investigate the surface dosed to saturation at ~100 °C. Figure 2a shows a filled state STM image after exposure for 260 min to P_2, with a step edge running diagonally across the image. The $p(2 \times 1)$ and $c(4 \times 2)$ reconstructions typical of clean Ge(001), as seen Figure 1a, are no longer visible. Instead, a complex surface structure is observed with a dense distribution of protrusions of different height and size. To unambiguously assign these features, a detailed study of coadsorption effects arising by the balance between various adsorbate−adsorbate and adsorbate−surface interactions is required, which goes beyond the scope of this article. We find, however, that extended domains of local ordering are present on the surface, such as that one highlighted in the inset of Figure 2a, where pairing of protrusion on a single dimer is similar to that observed for a $P_{2,b}$ rather than a $P_{2,a}$ feature in Figure 1. As a result, the adsorption configuration where P−P bonds are parallel to Ge dimers is more prominent at high coverage compared to what was observed in the low-coverage experiment, therefore yielding to chemisorption of P atoms on the surface exceeding half monolayer coverage.

Figure 2b shows a filled state STM image of the saturated Ge surface after a 5 min anneal to 360 °C to drive P incorporation. We may describe the surface in analogy with the P/Si(001) at high P coverages,[28] due to the striking similarity in atomic-resolution STM imaging (compare Figure 2a with Figures 2, 3, and 11 of ref 28). Near monolayer P coverage, Ge(001) is primarily saturated with P−P dimers with P−P bond parallel to the Ge dimer bond. Within a single 2×1 unit cell (Figure 2c and schematics), P atoms are clearly resolved into two protrusion, in contrast with the "bean-like" shape typical of unbuckled clean Ge dimers (Figure 1a,c). Occasionally, Ge−P heterodimers are present, in which Ge atoms appear as bright, round protrusions sitting higher on one side of the Ge−P heterodimer and P atoms appear as dark depressions. Two-dimensional islands as observed in Figure 1b are not formed because, in this case, the longer incorporation anneal (5 min *vs* 1 s) at higher temperatures (360 °C *vs* 250 °C) drives diffusion of the ejected Ge atoms on the surface leading to their attachment at monatomic step edges (see Supporting Information). On a larger scale, we note the presence in Figure 2b of low-rising darker segments. These extended line defects act as a strain−relief mechanism, allowing for lateral expansion of the surface layer and helping to stabilize the surface against the tensile stress arising from the expected shorter P−P bond in P dimers compared to the Ge−Ge bond. Two-dimensional Fourier transforms of STM images of the surface before and after saturation with P−P dimers (Figure 2d,e, respectively) highlight the different surface reconstructions, as they evolve from a 2×1 type, typical of clean Ge(001), to a 1×1 type due to P atoms in P−P dimers resolved into bright protrusions.

Structural Characterization by SIMS. To determine the maximal doping density in Ge using P_2 as precursor, we studied the structural and electrical properties of

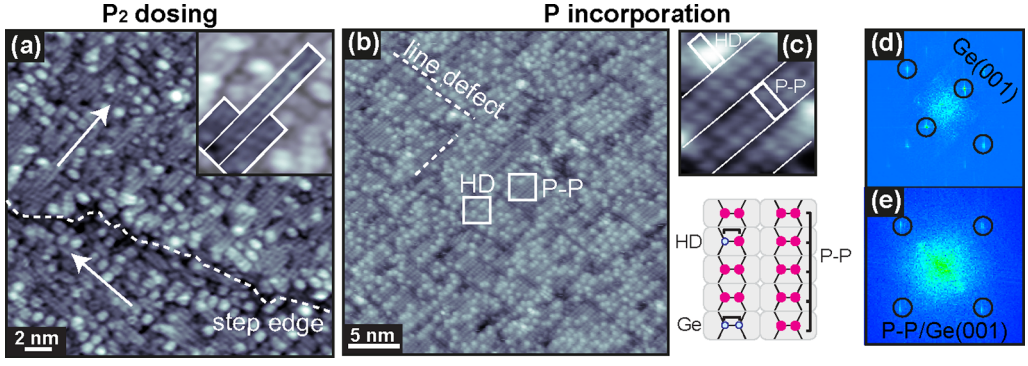

Figure 2. (a) Ge(001) surface after saturation dosing by 260 min exposure to P_2 flux at T_{SUB} = 100 °C. The dimer row directions are indicated for clarity with arrows. Inset highlights domains of local ordering on the surface. (b,c) After thermal incorporation at T_{SUB} = 360 °C, the Ge(001) is primarily saturated with P−P dimers while only a few Ge:P heterodimers are present. (d,e) Two-dimensional Fourier transforms of STM images of the surface before and after saturation with P−P dimers highlight (2×1) and (1×1) surface reconstructions arising from clean Ge(001) and P−P saturated Ge(001), respectively.

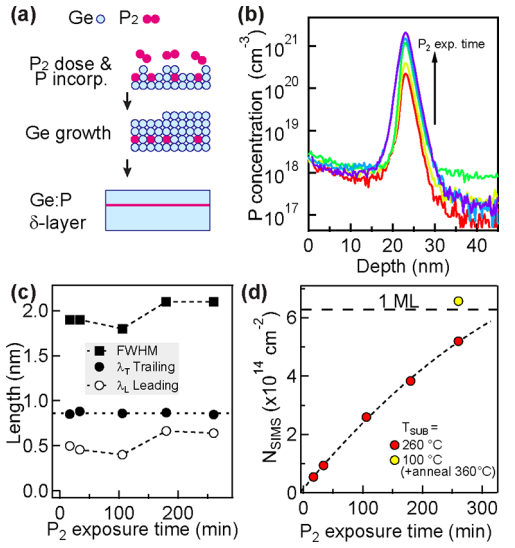

Figure 3. Structural characterization of P δ-layers. (a) Fabrication process schematics, (b) SIMS depth profiles of sharp and narrow δ-layers with different P_2 exposure time, (c) SIMS peaks analysis of full width at half-maximum, trailing and leading exponential edges showing very little segregation and diffusion. (d) Total concentration of P atoms incorporated in the δ-layers obtained by integrating the SIMS depth profiles.

different P δ-layers in which we progressively increased the P_2 exposure time. The δ-layers were obtained by incorporation of P layers into Ge(001) followed by encapsulation with a 25 nm thick Ge layer deposited by MBE (Figure 3a, schematics). The entire fabrication process was carried out at a constant substrate temperature $T_{SUB} = 250$ °C. The advantage of this process design choice is two-fold: as shown above, $T_{SUB} = 250$ °C guarantees full P incorporation; at this temperature, moreover, Ge overgrowth locks the P δ-layer in the crystalline matrix while minimizing dopant redistribution, observed above 460 °C in Ge:P δ-layers from PH_3.[14] Moreover, choosing such a single-process temperature greatly simplifies scaling up the process by multiple δ-doping cycles.

The P dopant distribution (Figure 3b) was investigated *ex situ* by SIMS. The sharp and narrow peaks ~25 nm below the surface are due to the confinement of P atoms on the starting Ge surface during he encapsulation process. The concentration at peak maximum increases monotonically from $\sim 10^{20}$ to $\sim 10^{21}$ cm^{-3} upon increasing the exposure time. A detailed analysis of SIMS peak shape is provided in Figure 3c. The peak full width at half-maximum (fwhm) along with the leading (λ_L) and trailing (λ_T) exponential slopes does not follow a particular trend upon increasing the P_2 exposure time, indicating that at $T_{SUB} = 250$ °C negligible dopant redistribution has occurred during prolonged exposure to P_2. All profiles are skewed away from the surface with $\lambda_T > \lambda_L$ due to the SIMS artifact from ion beam mixing in the sputtering process. By taking the average value $\langle\lambda_L\rangle = 0.540 \pm 0.10$ nm/e as an upper bound estimate for segregation length during overgrowth, we conclude that very little segregation occurs in the fabrication of these δ-layers, in agreement with that observed using PH_3 dopant molecules.[14]

The total concentration of P atoms (N_{SIMS}) incorporated in the δ-layers was measured by integrating the depth profiles in Figure 3b. An exposure time of 260 min provides 0.82 ML of P rather than the near monolayer expected from extrapolating the doping rate of 0.21 ML at short exposure times, pointing to a Langmuir-type kinetics for the P incorporation reaction at 250 °C. Indeed, a near monolayer of incorporated P was achieved, for the same exposure time, for the sample characterized previously in Figure 2, which was first dosed at a substrate temperature of 100 °C, therefore providing a maximal P coverage on the surface, and then annealed to 360 °C to incorporate P atoms (Figure 3d, additional yellow circle).

Electrical Characterization. The ability to tune the doping density from very low to very high coverage allows us to gain an insight into the electrical properties of P-doped layers. Previous studies on Ge:P δ-doped layers obtained using PH_3 as dopant precursor were limited to a maximum P concentration of 0.4 ML, and thus the investigation of the deactivation process in the high density regime was hindered so far.[14] The electrical properties of the Ge:P δ-doped layers obtained by P_2 (dopant profiles in Figure 3b) were investigated by four terminal magnetotransport measurements on trench-isolated Hall bars using standard low-frequency lock-in techniques. The measurements of transverse Hall resistance (ρ_{xy}) and sheet resistivity (ρ_{xx}) were performed at 4.2 K in liquid He to freeze-out bulk conduction through the lightly doped substrate. All samples showed similar trends in the magnetotransport measurements. Ohmic conduction was obtained at 4.2 K due to high doping level above the metal−insulator transition. The electron density n_{Hall} was calculated from the slope of the linear dependence of ρ_{xy} *versus* perpendicular magnetic field B. The sheet resistivity ρ_{xx} showed a peak at $B = 0$ magnetic field due to weak localization of electrons coherently backscattered in time-reversed trajectories. Observation of weak localization highlights the 2D nature of transport in the electron gas obtained by the strong vertical confinement of the dopants, in agreement with SIMS measurements.

In Figure 4a, we show the 2D electron density n_{Hall} as a function of doping density dose N_{SIMS} as obtained by SIMS measurements. Full electrical activation (Figure 4a, dashed line) is observed up to a dopant concentration of $\sim 10^{14}$ cm^{-2} only (0.16 ML). Above this density, additional P dopants do not provide active carriers to the two-dimensional electron gas. This observation is in agreement with previous results on Ge:P δ-layers from PH_3,[14] pointing to a common origin of dopant deactivation. An insight into dopant

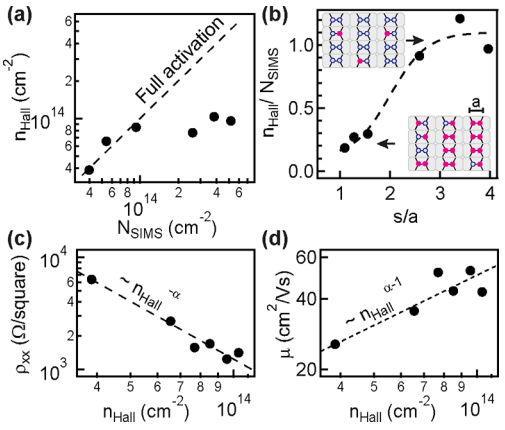

Figure 4. Electrical characterization of Ge:P δ-layers fabricated with different P_2 exposure time: (a) 2D electron density n_{Hall} as a function of doping density N_{SIMS} shows full activation only up to ~10^{14} cm^{-2}; (b) fraction of active dopants as a function of average dopant separation in the plane of the δ-layer, expressed in units of the Ge lattice site separation in the (001) surface. Insets show possible P atom configurations in the plane of the δ-layer at low and high doping density. (c) Sheet resistivity and (d) electron mobility as a function of 2D electron density point to an increment of transport qualities due to screened Coulomb scattering from ionized impurities.

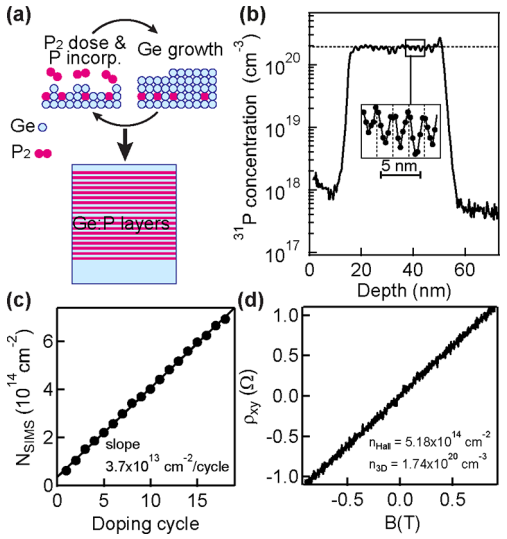

Figure 5. Atomically abrupt box-like shaped dopant profile obtained by repeated δ-doping cycles: (a) process schematics, (b) SIMS P depth profile, (c) accumulated P density at each doping cycle highlighting the robustness and reproducibility of the doping process, (d) transverse Hall resistance from which a high 3D electron density of 1.74 × 10^{20} cm^{-3} is estimated.

activation is provided in Figure 4b. Here we have plotted the fraction of active dopants (n_{Hall}/N_{SIMS}) against the average dopant separation s in the plane of the δ-layer, expressed in units of the Ge lattice site separation in the (001) surface (a = 0.4 nm). The average dopant separation was estimated as $s = 1/\sqrt{N_{SIMS}}$. We observe a trend characterized by two regimes of high and low activation (dashed line is a guide for the eyes). On average, a large fraction of dopants are electrically active when they are separated more than two lattice sites. In terms of dopant configurations in the plane, this means that P atoms along the same dimer row are not sitting on neighboring dimers. A cartoon of a possible P configuration within the plane is shown in the top left corner of Figure 4b, corresponding to a P coverage of 0.125 ML (P separation s/a ~2.8). In this configuration, electrically active P atoms—well-separated from each other—are incorporated into the surface only as Ge−P heterodimers. This is what we observe in STM images presented in Figure 1b,d. In contrast, a likely P configuration in the low-activation regime is shown in the bottom right corner of Figure 4b, corresponding to P coverage of 0.75 ML (s/a ~1.15). As dopants are brought closer, due to their proximity, they are likely to form P−P dimers such as those seen in Figure 2c that act as deactivating dopant complexes. Here only the minor fraction of P atoms arranged in Ge−P heterodimers will contribute to electron transport.

To understand the scattering mechanism limiting the electron transport in the δ-doped samples, the density-dependent resistivity ρ_{xx} and electron mobility μ are shown in Figure 4c,d, respectively. The resistivity decreases monotonically with electron density following a power law $\rho_{xx}(0) \propto n_{Hall}^{-\alpha}$ with $\alpha \sim 1.7$. This exponent is close to the value of 1.5 expected for screened Coulomb scattering from the ionized impurities. Because $\alpha > 1$, the mobility, instead, increases with n_{Hall} since

$$\mu = [\rho_{xx}(0) e n_{Hall}]^{-1} \propto n_{Hall}^{\alpha - 1} \quad (1)$$

A trend of increasing mobility with carrier density is in agreement with recent calculations for Ge:P δ-doped layers in the high-density weak-screening regime.[29] The experimental mobility is, however, much smaller than the upper limits provided theoretically. As suggested in ref 29, this points out additional scattering from other sources of disorder, such as structural disorder, possibly originating in our case from Ge overgrowth at 250 °C.

Multiple δ-Doping. The viability of δ-doping with P_2 molecules to produce highly doped and electrically active Ge films is demonstrated by fabricating a proof of principle sample with 18 δ-layer closely stacked in the Ge crystal (interlayer separation 2.2 nm). A schematic of the fabrication process is shown in Figure 5a. On the basis of the knowledge gained from the electrical characterization of the single δ-layers, we designed the P_2 exposure step to provide in each layer a doping density of ~5 × 10^{13} cm^{-2}, a reasonable compromise between full dopant activation and overall fabrication times considering the slow doping rate of the process. The substrate temperature was kept constant at T_{SUB} = 250 °C throughout the repeated doping cycles.

The P profile measured by SIMS (Figure 5b and inset therein) shows 18 closely spaced peaks confined in a box-like shape with atomically sharp leading and trailing edges of $\lambda_L = 0.6$ nm and $\lambda_T = 0.84$ nm, respectively. The total P areal dose incorporated in the thin film was $N_{SIMS} = 6.95 \times 10^{14}$ cm^{-2} with an average 3D doping concentration of 1.84×10^{20} cm^{-3} and a fwhm of 36.5 nm. The trailing edge of the multilayer is the same as in a single δ-layer grown under the same conditions (Figure 3b, red curve). This gives a strong indication that minimal dopant diffusion has occurred as a consequence of the multiple doping cycles. The leading edge has slightly increased (0.61 nm *versus* 0.50 nm), indicating the presence of a growing front of segregated P accumulating at each doping cycle throughout the very thin Ge spacer layer. Figure 5c shows the P density accumulated into the layer at each doping cycle obtained by integrating the profile in Figure 5a from peak to peak. The perfectly linear relationship observed in Figure 5c highlights the robustness and reproducibility of the doping process. The same amount of phosphorus is incorporated at each doping cycle. The average doping concentration per layer is 3.8×10^{13} cm^{-2}, less than 5×10^{13} cm^{-2} measured in the reference single δ-layer, because of limited segregation occurring at each doping cycle.

The electrical properties of the multilayer stack were measured at 4.2 K as for the single δ-layers. Figure 5d shows the linear relationship of the transverse resistance *versus* magnetic field from which a 2D electron density $n_{Hall} = 5.18 \times 10^{14}$ cm^{-2} is calculated. This corresponds to a 3D electron density of 1.74×10^{20} cm^{-3} assuming the doping profile fwhm as the layer thickness. The fraction of active dopants n_{Hall}/N_{SIMS} has reduced from unity to 0.75 as a consequence of repeated δ-doping. Quite significantly, we found a low resistivity of 120 Ω/square corresponding to a mobility of ~100 cm^2/(V s). This is a drastic ~3× improvement in mobility compared to the single δ-layer grown under similar conditions. We speculate that the reasons for such improvement are two-fold. First, repeated annealing due to multiple stacking increases the overall crystal quality, thereby reducing additional scattering mechanisms. In addition, the band structure of the multiple stacked layers will be substantially different from the single-layer case with electron wave functions being delocalized in the interlayer region between the very close quantum wells. Electrons therefore experience less scattering from the ionized impurities, similar to modulation doping.

CONCLUSIONS

In summary, we harness the smaller footprint of P_2 compared to PH_3 on Ge(001) to achieve tunable δ-doping with near-monolayer P coverage. By resolving the density-dependent doping process at the atomic level, we reveal the origin of dopant deactivation at high P coverages. Combining this knowledge with the unique properties of Ge to achieve high crystal quality growth at relatively low temperature, we demonstrated stacking of δ-doped layers obtained by P_2 while preserving high donor activation and electron densities. This technology has the potential to precisely control thickness and electron concentrations over a wide range in doped Ge films, overcoming one of the major challenges that has limited the development of a Ge-on-Si laser to date.

METHODS

Sample Preparation. All samples were fabricated in a customized ultrahigh vacuum system (base pressure $<5 \times 10^{-11}$ mbar) comprising a MBE system (MBE Komponenten) for Ge deposition and P_2 dosing (minimum sample temperature ~100 °C), an STM system (Omicron GmbH) for imaging at room temperature, and an additional chamber for surface preparation. The three chambers are connected *via* UHV transfer chambers.

Ge(001) samples 2.5×10 mm^2 in size were cleaved from a Sb-doped Ge(001) 4 in. wafer (resistivity of 1−10 Ω·cm). Light doping was required for STM imaging. Atomically flat, clean, and defect-free Ge(001) surfaces were prepared according to the method described in detail in ref 30. This method combines combines an *ex situ* wet chemical cleaning treatment using HCl/H_2O (36:100) and H_2O_2/H_2O (7:100) to alternately strip and reform a GeO_x passivation layer, with an *in situ* cleaning treatment which involves a controlled *in situ* thermal desorption of the oxide layer by flash-anneal at 760 °C followed by a 25 nm Ge buffer layer growth by MBE at a rate of ~0.15 Å/s and sample temperature of 500 °C and a subsequent final thermal anneal at 760 °C.

For P doping, a beam of P_2 molecules was sourced in the MBE chamber from a commercially available GaP cell (Deco-D phosphorus doping source, MBE Komponenten) operated at 700 °C and equipped with a dedicated shutter to minimize background doping. The concentration of gallium incorporated in the doped films, as measured by SIMS profiling, was in the 10^{16}−10^{17}cm^{-3} range and 4 orders of magnitude less than the incorporated phosphorus.

Final encapsulation Ge layers embedding the P layers in the Ge crystal were grown by MBE at a sample temperature of 250 °C to minimize dopant diffusion and segregation.

Depth Profiling. After removal from UHV, Ge:P-doped layer samples were cleaved and shipped to EAG (Evans Analytical Group) for an independent characterization by secondary ions mass spectroscopy. The ^{31}P profiles were carried out with a Quadrupole SIMS instrument with a low-energy 1 keV Cs^+ primary ion impact at 60° angle of incidence beam to optimize depth resolution.

Electrical Characterization. Trench-isolated Hall bar structures to investigate the electrical properties of the doped layers were defined by a CHF_3/CF_4-based dry etch with thermally evaporated Al Ohmic contacts connecting the P δ-doped layers or all multiple P layers of the δ-doped stack. The electrical measurements were performed at 4.2 K using a dipstick in liquid helium equipped with a superconducting magnet providing a perpendicular magnetic field up to 1 T. Four-terminal magnetotransport characterization was performed using standard low-frequency techniques employing Stanford SR830 lock-ins and injection currents of ~100 nA to measure simultaneously the perpendicular magnetic field B dependence of the longitudinal ρ_{xx} and transverse ρ_{xy} component of the resistivity tensor where x and y are, respectively, the directions parallel or perpendicular to the current flow in the Hall bar.

Conflict of Interest: The authors declare no competing financial interest.

Acknowledgment. G.M. and G.C. acknowledge support from UNSW. G.S. acknowledges support from the ARC (project number DP130100403). M.Y.S. acknowledges an Australian Government Federation Fellowship.

Supporting Information Available: Additional STM investigation of surface morphology after P incorporation as a function of process thermal budget and P coverage. This material is available free of charge *via* the Internet at http://pubs.acs.org.

REFERENCES AND NOTES

1. Michel, J.; Liu, J. F.; Kimerling, L. C. High-Performance Ge-on-Si Photodetectors. *Nat. Photonics* **2010**, *4*, 527–534.
2. Liu, J.; Beals, M.; Pomerene, A.; Bernardis, S.; Sun, R.; Cheng, J.; Kimerling, L. C.; Michel, J. Waveguide-Integrated, Ultralow-Energy GeSi Electro-absorption Modulators. *Nat. Photonics* **2008**, *2*, 433–437.
3. Liang, D.; Bowers, J. E. Recent Progress in Lasers on Silicon. *Nat. Photonics* **2010**, *4*, 511–517.
4. Virgilio, M.; Manganelli, C. L.; Grosso, G.; Pizzi, G.; Capellini, G. Radiative Recombination and Optical Gain Spectra in Biaxially Strained n-Type Germanium. *Phys. Rev. B* **2013**, *87*, 235313.
5. Liu, J. F.; Sun, X. C.; Camacho-Aguilera, R.; Kimerling, L. C.; Michel, J. Ge-on-Si Laser Operating at Room Temperature. *Opt. Lett.* **2010**, *35*, 679–681.
6. Camacho-Aguilera, R. E.; Cai, Y.; Patel, N.; Bessette, J. T.; Romagnoli, M.; Kimerling, L. C.; Michel, J. An Electrically Pumped Germanium Laser. *Opt. Express* **2012**, *20*, 11316–11320.
7. Boucaud, P.; El Kurdi, M.; Ghrib, A.; Prost, M.; de Kersauson, M.; Sauvage, S.; Aniel, F.; Checoury, X.; Beaudoin, G.; Largeau, L.; *et al.* Recent Advances in Germanium Emission [Invited]. *Photonics Res.* **2013**, *1*, 102–109.
8. Dutt, B.; Sukhdeo, D. S.; Nam, D.; Vulovic, B. M.; Yuan, Z.; Saraswat, K. C. Roadmap to an Efficient Germanium-on-Silicon Laser: Strain *vs.* n-Type Doping. *IEEE Photonics J.* **2012**, *4*, 2002–2009.
9. Gaubas, E.; Vanhellemont, J.; Simoen, E.; Romandic, I.; Geens, W.; Clauws, P. Carrier Lifetime Dependence on Doping, Metal Implants and Excitation Density in Ge and Si. *Physica B* **2007**, *401*, 222–225.
10. Oehme, M.; Gollhofer, M.; Widmann, D.; Schmid, M.; Kaschel, M.; Kasper, E.; Schulze, J. Direct Bandgap Narrowing in Ge LED's on Si Substrates. *Opt. Express* **2013**, *21*, 2206–2211.
11. Chui, C. O.; Kulig, L.; Moran, J.; Tsai, W.; Saraswat, K. C. Germanium n-Type Shallow Junction Activation Dependences. *Appl. Phys. Lett.* **2005**, *87*, 091909.
12. Brotzmann, S.; Bracht, H. Intrinsic and Extrinsic Diffusion of Phosphorus, Arsenic, and Antimony in Germanium. *J. Appl. Phys.* **2008**, *103*, 033508.
13. Pillarisetty, R. Academic and Industry Research Progress in Germanium Nanodevices. *Nature* **2011**, *479*, 324–328.
14. Scappucci, G.; Capellini, G.; Simmons, M. Y. Influence of Encapsulation Temperature on Ge:P δ-Doped Layers. *Phys. Rev. B* **2009**, *80*, 233202.
15. Scappucci, G.; Capellini, G.; Klesse, W. M.; Simmons, M. Y. Phosphorus Atomic Layer Doping of Germanium by the Stacking of Multiple δ Layers. *Nanotechnology* **2011**, *22*, 375203.
16. Klesse, W. M.; Scappucci, G.; Capellini, G.; Hartmann, J. M.; Simmons, M. Y. Atomic Layer Doping of Strained Ge-on-Insulator Thin Films with High Electron Densities. *Appl. Phys. Lett.* **2013**, *102*, 151103.
17. Scappucci, G.; Capellini, G.; Klesse, W. M.; Simmons, M. Y. New Avenues to an Old Material: Controlled Nanoscale Doping of Germanium. *Nanoscale* **2013**, *5*, 2600.
18. Yu, H. Y.; Cheng, S. L.; Griffin, P. B.; Nishi, Y.; Saraswat, K. C. Germanium *In Situ* Doped Epitaxial Growth on Si for High-Performance n(+)/p-Junction Diode. *IEEE Electron Device Lett.* **2009**, *30*, 1002–1004.
19. Dilliway, G.; Van Den Boom, R.; Moussa, A.; Leys, F.; Van Daele, B.; Parmentier, B.; Clarysse, T.; Simoen, E. R.; Defranoux, C.; Meuris, M. M.; *et al. In Situ* Phosphorus Doping of Germanium by APCVD. *ECS Trans.* **2006**, *3*, 599–609.
20. Yamamoto, Y.; Kurps, R.; Mai, C.; Costina, I.; Murota, J.; Tillack, B. Phosphorus Atomic Layer Doping in Ge Using RPCVD. *Solid-State Electron.* **2013**, *83*, 25–29.
21. Scappucci, G.; Warschkow, O.; Capellini, G.; Klesse, W. M.; McKenzie, D. R.; Simmons, M. Y. n-Type Doping of Germanium from Phosphine: Early Stages Resolved at the Atomic Level. *Phys. Rev. Lett.* **2012**, *109*, 076101.
22. Scappucci, G.; Capellini, G.; Lee, W. C. T.; Simmons, M. Y. Ultradense Phosphorus in Germanium δ-Doped Layers. *Appl. Phys. Lett.* **2009**, *94*, 162106.
23. Lippert, G.; Osten, H. J.; Kruger, D.; Gaworzewski, P.; Eberl, K. Heavy Phosphorus Doping in Molecular-Beam Epitaxial Grown Silicon with a Gap Decomposition Source. *Appl. Phys. Lett.* **1995**, *66*, 3197–3199.
24. Goh, K. E. J.; Oberbeck, L.; Butcher, M. J.; Curson, N. J.; Ruess, F. J.; Simmons, M. Y. Comparison of GaP and PH_3 as Dopant Sources for STM-Based Device Fabrication. *Nanotechnology* **2007**, *18*, 065301.
25. Sagisaka, K.; Marz, M.; Fujita, D.; Bowler, D. Adsorption of Phosphorus Molecules Evaporated from an InP Solid Source on the Si(100) Surface. *Phys. Rev. B* **2013**, *87*, 155316.
26. Curson, N. J.; Schofield, S. R.; Simmons, M. Y.; Oberbeck, L.; O'Brien, J. L.; Clark, R. G. STM Characterization of the Si-P Heterodimer. *Phys. Rev. B* **2004**, *69*, 195303.
27. Scappucci, G.; Capellini, G.; Johnston, B.; Klesse, W. M.; Miwa, J. A.; Simmons, M. Y. A Complete Fabrication Route for Atomic-Scale, Donor-Based Devices in Single-Crystal Germanium. *Nano Lett.* **2011**, *11*, 2272–2279.
28. Wang, Y. J.; Chen, X. X.; Hamers, R. J. Atomic-Resolution Study of Overlayer Formation and Interfacial Mixing in the Interaction of Phosphorus with Si(001). *Phys. Rev. B* **1994**, *50*, 4534–4547.
29. Hwang, E. H.; Das Sarma, S. Electronic Transport in Two-Dimensional Si:P δ-Doped Layers. *Phys. Rev. B* **2013**, *87*, 125411.
30. Klesse, W. M.; Scappucci, G.; Capellini, G.; Simmons, M. Y. Preparation of the Ge(001) Surface towards Fabrication of Atomic-Scale Germanium Devices. *Nanotechnology* **2011**, *22*, 145604.